A ROTATED CHARACTERISTIC DECOMPOSITION TECHNIQUE FOR HIGH-ORDER RECONSTRUCTIONS IN MULTI-DIMENSIONS

A PREPRINT

Hua Shen *
School of Mathematical Science
University of Electronic Science and Technology of China
Chengdu, Sichuan, 611731, China
huashen@uestc.edu.cn

Matteo Parsani
Extreme Computing Research Center (ECRC)
Computer, Electrical and Mathematical Sciences & Engineering (CEMSE)
King Abdullah University of Science and Technology (KAUST)
Thuwal, 23955-6900, Kingdom of Saudi Arabia
matteo.parsani@kaust.edu.sa

May 24, 2021

ABSTRACT

When constructing high-order schemes for solving hyperbolic conservation laws, the corresponding high-order reconstructions are commonly performed in characteristic spaces to eliminate spurious oscillations as much as possible. For multi-dimensional finite volume (FV) schemes, we need to perform the characteristic decomposition several times in different normal directions of the target cell, which is very time-consuming. In this paper, we propose a rotated characteristic decomposition technique which requires only one-time decomposition for multi-dimensional reconstructions. The rotated direction depends only on the gradient of a specific physical quantity which is cheap to calculate. This technique not only reduces the computational cost remarkably, but also controls spurious oscillations effectively. We take a third-order weighted essentially non-oscillatory finite volume (WENO-FV) scheme for solving the Euler equations as an example to demonstrate the efficiency of the proposed technique.

Keywords characteristic decomposition · high-order schemes · hyperbolic conservation laws · WENO · finite volume

1 Introduction

The solution to a nonlinear hyperbolic conservation law may become discontinuous even when the initial conditions are sufficiently smooth. Therefore, the shock-capturing property is a desired feature of a numerical scheme for solving hyperbolic conservation laws. Usually, low-order schemes are more stable than high-order schemes for capturing discontinuities. However, in smooth regions, low-order schemes converge too slow, so they require a very fine mesh to achieve low-level errors. In many applications, discontinuities and sophisticated structures coexist, hence shock-capturing high-order schemes are preferred. In the development history of numerical schemes for solving hyperbolic conservation laws, the order of the numerical schemes gradually increased. Van Leer Van Leer [1979] proposed a second-order monotonic upstream-centered scheme for conservation laws (MUSCL) which is an extension of the first-order Godunov scheme Godunov [1959]. Colella and Woodward Colella and Woodward [1984] proposed a third-order piecewise parabolic method (PPM) which was extended from MUSCL. Harten and his coworkers Harten et al. [1987]

*This work was supported by the National Natural Science Foundation of China (Contract No. 11901602).

proposed a general framework to design uniformly high-order accurate essentially non-oscillatory (ENO) schemes by using the strategy of adaptively choosing the smoothest stencil from several local candidates. Liu *et al*. Liu et al. [1994] proposed weighted ENO (WENO) schemes by assigning a proper weight to each candidate stencil. Jiang and Shu Jiang and Shu [1996] improved the accuracy of WENO schemes by carefully design the weights. Borges *et al*. Borges et al. [2008] proposed WENO-Z schemes by further improving the weights for the candidate stencils. Levy, Puppo and Russo Levy et al. [1999, 2000a,b] proposed a class of central WENO (CWENO) schemes which reconstruct a single polynomial in the entire traget cell. Therefore, CWENO schemes are cheaper than standard WENO-FV schemes when there are many reconstruction points in a cell and can be trivially extended to the case of non-Cartesian meshes. A detailed literature review of CWENO schemes can be found in Cravero et al. [2019]. In principle, we can construct arbitrarily high-order ENO/WENO schemes, but the size of stencils increases as the order increases. This feature makes it unfriendly for their implementation on unstructured meshes, although we can do it, see for example Abgrall [1994], Hu and Shu [1999], Dumbser and Käser [2007]. To overcome the above shortcoming, some compact high-order schemes are constructed by increasing the internal degree of freedoms (DOFs). The representative of compact schemes is the discontinuous Galerkin (DG) scheme Reed and Hill [1973], Cockburn and Shu [1989], Cockburn et al. [1989, 1990], Cockburn and Shu [1998] that relies on nonlinear limiters to capture discontinuities, see for example Qiu and Shu [2004, 2005], Zhong and Shu [2013], Zhu et al. [2016]. Dumbser *et al*. Dumbser et al. [2008], Dumbser and Zanotti [2009], Dumbser [2010] proposed a class of $P_N P_M$ schemes which can flexibly choose the internal DOFs and reconstruction DOFs, thereby adjusting the compactness of the stencil.

When solving a hyperbolic system by ENO/WENO schemes or DG schemes with non-linear limiters, it is necessary to carry out reconstructions in characteristic space to control spurious oscillations Qiu and Shu [2002]. The reconstructions of multi-dimensional ENO/WENO finite difference (ENO/WENO-FD) schemes Shu and Osher [1988], Jiang and Shu [1996] can be efficiently performed in a dimension-by-dimension manner. However, ENO/WENO-FD only works for regular meshes. For irregular meshes, we have to resort to FV-type schemes, but classical ENO/WENO-FV schemes and DG schemes need to perform characteristic decomposition and reconstructions in all normal directions of the target cell. This is one of the major reasons that makes ENO/WENO-FV schemes more expensive than ENO/WENO-FD schemes in multi-dimensions. For Cartesian meshes, there are two and three normal directions in two- and three-dimensions, respectively. For unstructured meshes, there are even more normal directions than Cartesian meshes. In order to reduce the computational cost, some scholars proposed to only perform characteristic decomposition near discontinuities Ren et al. [2003], Puppo [2003], Puppo and Semplice [2011], Li and Qiu [2010], Peng et al. [2019]. This approach relies on a good switch function, otherwise the transition between non-characteristic reconstructions and characteristic reconstructions may become nonsmooth. In this paper, we introduce a rotated characteristic decomposition technique which requires only one-time characteristic decomposition in the direction of a physical quantity's gradient. This technique not only reduces the amount of computation significantly, but also can eliminate spurious oscillations effectively.

2 Description of the rotated characteristic decomposition technique

2.1 A brief review of WENO-FV schemes

We consider the hyperbolic conservation law, equipped with certain initial conditions and boundary conditions, which can be expressed as

$$\frac{\partial \mathbf{U}}{\partial t} + \nabla \cdot \mathbf{F} = 0, \quad \mathbf{x} \in \Omega, \quad t \in [0, \infty), \tag{1a}$$

$$\mathbf{U}(\mathbf{x}, 0) = \mathbf{U}_0(\mathbf{x}), \quad \mathbf{x} \in \Omega, \tag{1b}$$

$$\mathbf{U}(\mathbf{x}, t) = \mathbf{U}_{\partial\Omega}(\mathbf{x}, t), \quad \mathbf{x} \in \partial\Omega, \quad t \in [0, \infty). \tag{1c}$$

A semi-discrete FV scheme for solving Eq. (1) can be written as

$$\frac{d\bar{\mathbf{U}}_i}{dt} = -\frac{1}{\Omega_i} \sum_{j=1}^{J} |\partial\Omega_{i,j}| \sum_{k=1}^{K} \omega_k \hat{\mathbf{F}}\left(\mathbf{x}_k^G\right) \cdot \mathbf{n}_{i,j}, \tag{2}$$

where Ω_i is the discrete cell, $\partial\Omega_{i,j}$ is the jth edge of Ω_i, $\mathbf{n}_{i,j}$ is the unit outward normal vector of $\partial\Omega_{i,j}$, $\mathbf{x}_k^G$ and ω_k are the Gaussian quadrature points and weights applied for the computation of the numerical flux on $\partial\Omega_{i,j}$. The numerical fluxes at the Gaussian quadrature points can be calculated by local Riemann solvers. Here, we use the local Lax–Friedrichs flux that is expressed as

$$\hat{\mathbf{F}}\left(\mathbf{x}_k^G\right) = \frac{1}{2}\left\{\mathbf{F}^+\left(\mathbf{x}_k^G\right) + \mathbf{F}^-\left(\mathbf{x}_k^G\right) - S_{i,j}\left[\mathbf{U}^+\left(\mathbf{x}_k^G\right) - \mathbf{U}^-\left(\mathbf{x}_k^G\right)\right]\right\}, \tag{3}$$

where $S_{i,j}$ is the local upper bound for the eigenvalues of the Jacobian in the $\mathbf{n}_{i,j}$ direction, $\mathbf{U}^{\pm}\left(\mathbf{x}_k^G\right)$ is interpolated from the target cell and the neighboring cell.

In order to get a pth-order scheme, we have to reconstruct a $(p-1)$th-order polynomial $\mathbf{U}_i(\mathbf{x})$ from cell averages to approximate the solution in every cell. A popular reconstruction method is WENO which is a nonlinearly convex combination of linear reconstructions on several local stencils. In this work, we take a two-dimensional third-order WENO-FV scheme on Cartesian meshes as an example to demonstrate the efficiency of the proposed technique. The WENO reconstructions proposed by Balsara *et al*. Balsara et al. [2009] is used for space reconstructions, and the third order TVD Runge–Kutta method Shu and Osher [1988] is adopted for time discretization. When constructing non-linear stencil weights, we use the smoothness measures to the second power and set $\epsilon = 10^{-40}$. The other settings exactly keep the same with those used by Balsara *et al*. Balsara et al. [2009].

2.2 The rotated characteristic decomposition technique for the two-dimensional Euler equations

We consider the two-dimensional Euler equations, namely

$$\frac{\partial \mathbf{U}}{\partial t} + \frac{\partial \mathbf{F}_1}{\partial x_1} + \frac{\partial \mathbf{F}_2}{\partial x_2} = 0, \tag{4a}$$

with

$$\mathbf{U} = \begin{bmatrix} \rho \\ \rho u \\ \rho v \\ \rho e \end{bmatrix}, \mathbf{F}_1 = \begin{bmatrix} \rho u \\ \rho u^2 + p \\ \rho uv \\ (\rho e + p)u \end{bmatrix}, \mathbf{F}_2 = \begin{bmatrix} \rho v \\ \rho uv \\ \rho v^2 + p \\ (\rho e + p)v \end{bmatrix}, \tag{4b}$$

where ρ is the density, u and v are respectively velocity component in x_1 and x_2 directions, p is the pressure, e is the specific total energy. For ideal gases, we have

$$e = \frac{p}{(\gamma-1)\rho} + \frac{1}{2}(u^2 + v^2). \tag{5}$$

The Jacobian matrix corresponding to $\mathbf{F}_1$ is

$$\mathbf{A}(\mathbf{U}) = \frac{\partial \mathbf{F}_1}{\partial \mathbf{U}} = \begin{bmatrix} 0 & 1 & 0 & 0 \\ \frac{\gamma-1}{2}K - u^2 & (3-\gamma)u & (1-\gamma)v & \gamma - 1 \\ -uv & v & u & 0 \\ \left(\frac{\gamma-1}{2}K - H\right)u & H - (\gamma-1)u^2 & (1-\gamma)uv & \gamma u \end{bmatrix}, \tag{6}$$

where $K = u^2 + v^2$, and $H = e + \frac{p}{\rho}$. The eigenvalues of $\mathbf{A}(\mathbf{U})$ are

$$\lambda_1 = u - a, \quad \lambda_2 = \lambda_3 = u, \quad \lambda_3 = u + a, \tag{7a}$$

of which the corresponding right eigenvectors are

$$\mathbf{r}_1 = \begin{bmatrix} 1 \\ u-a \\ v \\ H - au \end{bmatrix}, \mathbf{r}_2 = \begin{bmatrix} 1 \\ u \\ v \\ \frac{K}{2} \end{bmatrix}, \mathbf{r}_3 = \begin{bmatrix} 0 \\ 0 \\ 1 \\ v \end{bmatrix}, \mathbf{r}_4 = \begin{bmatrix} 1 \\ u+a \\ v \\ H + au \end{bmatrix}, \tag{7b}$$

where $a = \sqrt{\frac{\gamma p}{\rho}}$ is the sound speed. Define the right eigenvector matrix as $\mathbf{R} = [\mathbf{r}_1, \mathbf{r}_2, \mathbf{r}_3, \mathbf{r}_4]$, then the Jacobian matrix can be written as $\mathbf{A}(\mathbf{U}) = \mathbf{R}\mathbf{\Lambda}\mathbf{R}^{-1}$, where $\mathbf{\Lambda}$ is the diagonal matrix with $\mathbf{\Lambda}_{kk} = \lambda_k$, the left eigenvector matrix $\mathbf{R}^{-1}$ is expressed as

$$\mathbf{R}^{-1} = \frac{\gamma-1}{2a^2}\begin{bmatrix} \frac{au}{\gamma-1} + \frac{K}{2} & -\frac{a}{\gamma-1} - u & -v & 1 \\ \frac{2a^2}{\gamma-1} - K & 2u & 2v & -2 \\ -\frac{2a^2 v}{\gamma-1} & 0 & \frac{2a^2}{\gamma-1} & 0 \\ -\frac{au}{\gamma-1} + \frac{K}{2} & \frac{a}{\gamma-1} - u & -v & 1 \end{bmatrix}. \tag{8}$$

Once we get the flux and its eigenstructure in x_1 direction, we can use the rotational invariance property of the Euler equations to calculate the flux and the corresponding eigenstructure in an arbitrary direction, $\mathbf{n} = (n_1, n_2) = (cos\theta, sin\theta)$, as Toro [2013]

$$\mathbf{F}(\mathbf{U}, \theta) = cos\theta\mathbf{F}_1 + sin\theta\mathbf{F}_2 = \mathbf{T}^{-1}\mathbf{F}_1\left(\mathbf{T}\mathbf{U}\right), \tag{9a}$$

$$\mathbf{A}(\mathbf{U},\theta) = cos\theta\frac{\partial \mathbf{F}_1}{\partial \mathbf{U}} + sin\theta\frac{\partial \mathbf{F}_2}{\partial \mathbf{U}} = \mathbf{T}^{-1}\mathbf{A}\left(\mathbf{TU}\right)\mathbf{T}, \tag{9b}$$

$$\mathbf{R}(\mathbf{U},\theta) = \mathbf{T}^{-1}\mathbf{R}\left(\mathbf{TU}\right), \quad \mathbf{R}^{-1}(\mathbf{U},\theta) = \mathbf{R}^{-1}\left(\mathbf{TU}\right)\mathbf{T}, \tag{9c}$$

with the rotation matrix and its inverse defined as

$$\mathbf{T} = \begin{bmatrix} 1 & 0 & 0 & 0 \\ 0 & cos\theta & sin\theta & 0 \\ 0 & -sin\theta & cos\theta & 0 \\ 0 & 0 & 0 & 1 \end{bmatrix}, \mathbf{T}^{-1} = \begin{bmatrix} 1 & 0 & 0 & 0 \\ 0 & cos\theta & -sin\theta & 0 \\ 0 & sin\theta & cos\theta & 0 \\ 0 & 0 & 0 & 1 \end{bmatrix}. \tag{9d}$$

When we apply WENO schemes to solve the Euler equations, we have to perform all the reconstructions in characteristic space to eliminate spurious oscillations as much as possible. In standard WENO approaches, before we calculate the flux in $\mathbf{n}_{i,j} = (cos\theta_{i,j}, sin\theta_{i,j})$ direction in Eq. (2), we need the following three major steps in advance:

Step 1. Project the cell averages $\bar{\mathbf{U}}_m$ within the reconstruction stencils of the target cell Ω_i to local characteristic space, i.e., $\bar{\mathbf{U}}^{(c)}_{m,j} = \mathbf{R}^{-1}(\bar{\mathbf{U}}_i, \theta_{i,j})\bar{\mathbf{U}}_m$;

Step 2. Perform WENO reconstruction based on $\bar{\mathbf{U}}^{(c)}_{m,j}$, i.e., $\mathbf{U}^{(c)}_{i,j}(\mathbf{x}) = WENOREC\left(\bar{\mathbf{U}}^{(c)}_{m,j}\right)$;

Step 3. Transform $\mathbf{U}^{(c)}_{i,j}(\mathbf{x})$ back to physical space, i.e., $\mathbf{U}_{i,j}(\mathbf{x}) = \mathbf{R}(\bar{\mathbf{U}}_i, \theta_{i,j})\mathbf{U}^{(c)}_{i,j}(\mathbf{x})$.

Note that, we need to repeat N times the above steps on a target cell with N different normal directions. For example, on two-dimensional Cartesian meshes, we need to execute the above steps in x_1 and x_2 respectively.

In order to improve the efficiency, we propose a rotated characteristic decomposition technique which contains the following steps:

Step 1. Determine the rotated direction as $\hat{\mathbf{n}}_i = (cos\hat{\theta}_i, sin\hat{\theta}_i)$ with

$$cos\hat{\theta}_i = \frac{\rho_{x_1,i} + \epsilon}{\sqrt{(\rho_{x_1,i} + \epsilon)^2 + (\rho_{x_2,i} + \epsilon)^2}}, sin\hat{\theta}_i = \frac{\rho_{x_2,i} + \epsilon}{\sqrt{(\rho_{x_1,i} + \epsilon)^2 + (\rho_{x_2,i} + \epsilon)^2}}, \tag{10}$$

where the spatial derivatives $\rho_{x_1,i}$ and $\rho_{x_2,i}$ are calculated by central differences, and $\epsilon = 10^{-40}$ is a small number used to avoid singularity;

Step 2. Project the cell averages $\bar{\mathbf{U}}_m$ within the reconstruction stencils of the target cell Ω_i to local characteristic space, i.e., $\bar{\mathbf{U}}^{(c)}_m = \mathbf{R}^{-1}(\bar{\mathbf{U}}_i, \hat{\theta}_i)\bar{\mathbf{U}}_m$;

Step 3. Perform WENO reconstruction based on $\bar{\mathbf{U}}^{(c)}_m$, i.e., $\mathbf{U}^{(c)}_i(\mathbf{x}) = WENOREC\left(\bar{\mathbf{U}}^{(c)}_m\right)$;

Step 4. Transform $\mathbf{U}^{(c)}_i(\mathbf{x})$ back to physical space, i.e., $\mathbf{U}_i(\mathbf{x}) = \mathbf{R}(\bar{\mathbf{U}}_i, \hat{\theta}_i)\mathbf{U}^{(c)}_i(\mathbf{x})$.

At the first glance, the rotated characteristic decomposition technique requires one more step than the standard technique. However, the additional step to determine the rotated direction is very cheap, and the rotated characteristic decomposition technique always requires only one-time characteristic decomposition regardless of the number of the normal directions of the target cell. Therefore, the rotated characteristic decomposition technique can significantly reduce the computational cost comparing to the standard technique. Furthermore, spurious oscillations usually appear in the direction of shocks and contact discontinuities which can be detected by the density gradient, so we can effectively control the spurious oscillations by performing characteristic decomposition in the direction of the density gradient.

3 Numerical examples

We serially run all the simulations on a laptop equipped with Intel(R) Core(TM)i7-4720HQ CPU@2.60GHz. In all simulations, we set $CFL = 0.8$ and $\gamma = 1.4$. In this section, we respectively denote no characteristic decomposition as NCD, standard characteristic decomposition as SCD, and rotated characteristic decomposition as RCD for short. We note that, we perform RCD in the density gradient direction and the total energy gradient direction respectively, but no difference was observed. Therefore, we show only the results of RCD in the density gradient direction.

3.1 Isentropic vortex evolution

This case is used to demonstrate the effect of the RCD technique on smooth flows. The computational domain is $[-5, 5] \times [-5, 5]$ of which all boundaries are periodic. Initially, the mean flow ($\rho = 1, p = 1$ and $(u, v) = (1, 1)$) is disturbed by an isentropic vortex which is described by

$$(\delta u, \delta v) = \frac{\psi}{2\pi}e^{0.5(1-r^2)}(-y, x), \quad \delta T = -\frac{(\gamma - 1)\psi^2}{8\gamma\pi^2}e^{(1-r^2)}, \quad \delta S = 0, \tag{11}$$

Table 1: The density errors, convergence rates, and computational costs of the third-order WENO-FV scheme for the isentropic vortex evolution problem.

WENO-FV with NCD					
cell number	L_1	Order	L_∞	order	CPU time (s)
50×50	4.94E-4	-	7.74E-3	-	0.8
100×100	6.89E-5	2.84	9.32E-4	3.05	5.8
150×150	2.13E-5	2.90	2.34E-4	3.41	19
200×200	9.51E-6	2.80	1.00E-4	2.96	45
WENO-FV with SCD					
cell number	L_1	Order	L_∞	order	CPU time (s)
50×50	4.99E-4	-	7.78E-3	-	2
100×100	6.87E-5	2.86	9.14E-4	3.09	16
150×150	2.12E-5	2.90	2.29E-4	3.41	52
200×200	9.49E-6	2.79	1.01E-4	2.85	123
WENO-FV with RCD					
cell number	L_1	Order	L_∞	order	CPU time (s)
50×50	5.01E-4	-	7.72E-3	-	1.2
100×100	6.87E-5	2.87	9.17E-4	3.07	9
150×150	2.12E-5	2.90	2.31E-4	3.40	30
200×200	9.49E-6	2.79	1.01E-4	2.88	70

where $r^2 = x^2 + y^2$, $S = p/\rho^\gamma$ is the entropy, $T = p/\rho$ is the temperature, and ψ is the vortex strength. In our computations, we set $\psi = 5$.

The exact solution of this problem can be portrayed by the vortex moving at the mean velocity. We use the third-order WENO scheme with different characteristic decomposition techniques to compute this problem to $t = 2$. Table 1 shows the corresponding density errors, convergence rates, and computational costs. As we can see, the RCD technique has no effect on the accuracy of the scheme, but it significantly reduces CPU times as comparing with the SCD technique.

3.2 Double Mach reflection problem

This problem was proposed by Woodward and Colella Woodward and Colella [1984]. The computational domain is $[0, 4] \times [0, 1]$. At $t = 0$, an oblique Mach 10 shock is inclined at an angle of 60° to the horizontal direction. The pre-shock and post-shock states are given by

$$(\rho, u, v, p) = \begin{cases} (1.4, 0, 0, 1) & \text{if } x > \frac{1}{6} + \frac{y}{\sqrt{3}}, \\ (8, 8.25sin(60^\circ), -8.25cos(60^\circ), 116.5), & \text{otherwise.} \end{cases} \tag{12}$$

The post-shock states are imposed on the left boundary, and nonreflective boundary conditions are applied to the right boundary. On the top, the time-dependent boundary conditions are determined by the exact motion of the oblique shock. On the bottom, outflow conditions are imposed for $x \leq \frac{1}{6}$, and reflective boundary conditions are imposed for $x > \frac{1}{6}$.

This problem is equivalent to a horizontally moving Mach 10 shock reflects by a 60° wedge. Under current condition, a double Mach reflection will occur. We run this problem by the third-order WENO-FV scheme with 1920×480 cells up to $t = 0.28$. The CPU times of WENO-FV with NCD, SCD, and RCD are 18925s, 54032s, and 32179s, respectively. Fig. 1 shows the entire view of the density contours, and Fig. 2 shows the corresponding enlarged view. As we expected, the WENO-FV with NCD cannot control spurious oscillations effectively. The RCD technique can control oscillations well with a significantly less CPU time than the SCD technique. Meanwhile, the RCD and NCD techniques achieve similar resolutions for the complex slip line instability, as shown by Fig. 2.

3.3 Shock reflection on a plate

This is a steady-state shock reflection problem which was proposed by Yee *et al*. Yee et al. [1985]. The computational domain is $[0, 4] \times [0, 1]$ which is initialized by $(\rho, u, v, p) = (1, 2.9, 0, 1/\gamma)$. Non-reflective boundary conditions are imposed on the right, and reflective boundary conditions are imposed on the bottom. On the left and top, we impose

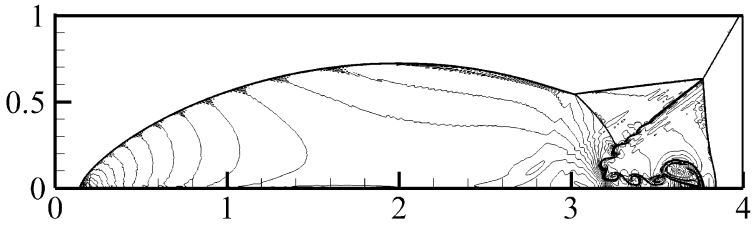

(a) WENO-FV with NCD

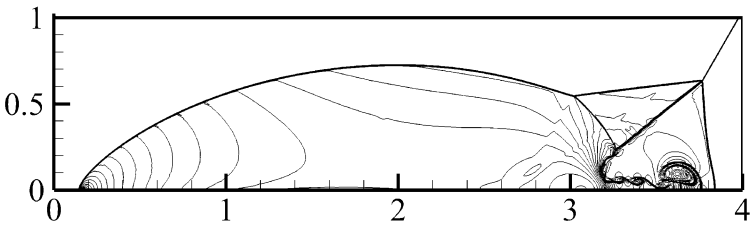

(b) WENO-FV with SCD

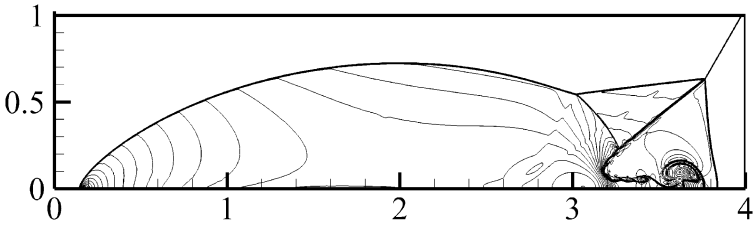

(c) WENO-FV with RCD

Figure 1: The entire view of the density contours of the double Mach reflection problem at $t = 0.28$ calculated by the third-order WENO-FV scheme with different characteristic decomposition techniques. The mesh size is 1/480 and the density contours contain 50 equidistant contours from 2 to 22.

the following Dirichlet boundary conditions

$$(\rho, u, v, p) = \begin{cases} (1, 2.9, 0, 1/\gamma) & \text{on the left,} \\ (1.69997, 2.61934, -0.50632, 1.52819)\,, & \text{on the top.} \end{cases} \tag{13}$$

We calculate this problem by the third-order WENO-FV scheme with 200×50 cells up to $t = 15$. The CPU times of WENO-FV with NCD, SCD, and RCD are 220s, 598s, and 358s, respectively. Fig. 3 shows the density contours, and Fig. 4 shows the corresponding density profiles along the line $y = 0.5$. Again, obvious oscillations are observed near the shocks calculated by the WENO-FV scheme with NCD. It is interesting to observe that RCD controls spurious oscillations better than SCD does. In Fig. 4(b), slight oscillations can also be observed in the density profile along the line $y = 0.5$ derived by the WENO-FV scheme with SCD. In contrast, oscillations are invisible in the density profile derived by the WENO-FV scheme with RCD. In order to confirm the embedded mechanism, we additionally perform the characteristic decomposition in x direction (xCD) and y direction (yCD). We observe that yCD achieves better results than xCD does, but slight oscillations near the reflected shock still exist as shown by Fig. 4(e). Since y direction is closer to the normal direction of the shock than x direction is, we conclude that the good outcome of RCD comes from the fact that the shock is oblique with respect to the grid and RCD works in the direction normal to it. Furthermore, we compare the maximum residual histories of the third-order WENO-FV scheme with different characteristic decomposition techniques in Fig. 5. Here, the maximum residual is calculated by $R^n_{max} = MAX(R^n_1, R^n_2, R^n_3, R^n_4)$ where $R^n_k = MAX \left| U^n_k - U^{n-1}_k \right|$ $(k = 1 \text{ to } 4)$ for all cells. As we can see from Fig. 5, the WENO-FV scheme with RCD has smaller residual oscillations than the WENO-FV scheme with NCD and SCD do, and the WENO-FV scheme with yCD has smaller residual oscillations than the WENO-FV scheme with xCD does. We note that, the residuals cannot achieve machine zero regardless of the characteristic decomposition technique. This is caused by the WENO reconstruction technique. If we want to reduce the residuals to machine zero, we have to use other technique, see for example the work of Zhu and Shu Zhu and Shu [2017].

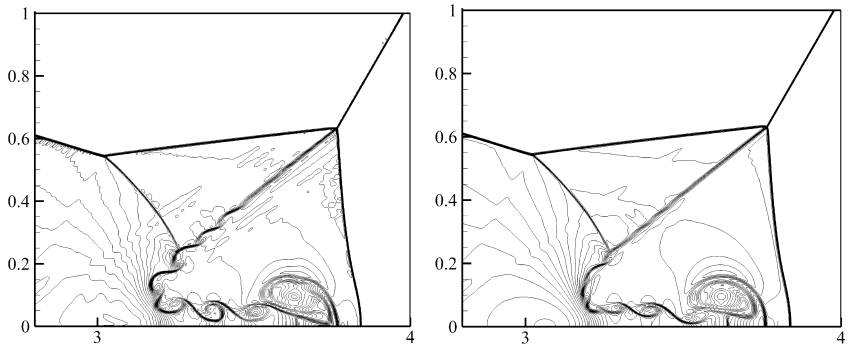

(a) WENO-FV with NCD (b) WENO-FV with SCD

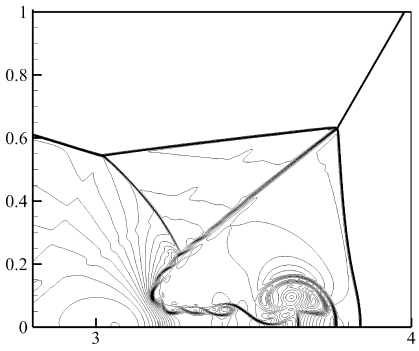

(c) WENO-FV with RCD

Figure 2: The enlarged view of the density contours of the double Mach reflection problem at $t = 0.28$ calculated by the third-order WENO-FV scheme with different characteristic decomposition techniques. The mesh size is 1/480 and the density contours contain 50 equidistant contours from 2 to 22.

4 Conclusions

We propose a rotated characteristic decomposition technique for high-order reconstructions in multi-dimensions. The third-order WENO-FV scheme with the proposed technique for the Euler equations can eliminate spurious effectively with about 40% less CPU times than the standard characteristic decomposition technique. For the steady shock reflection problem, the rotated characteristic decomposition technique achieves a even better performance than the standard characteristic decomposition technique does. The proposed technique can apply to other hyperbolic systems and other numerical methods relying on reconstructions. It is also easy to extend to three-dimensional and unstructured computations. Moreover, since the rotated characteristic decomposition technique requires only one-time characteristic decomposition regardless the number of normal directions of the mesh, it can save more CPU times for the three-dimensional and unstructured computations than the current Cartesian computations in two dimensions. If we want to further reduce the computational cost, we can employ the current approach in addition to the existing ones that only perform characteristic decomposition near discontinuities Ren et al. [2003], Puppo [2003], Puppo and Semplice [2011], Li and Qiu [2010], Peng et al. [2019].

References

Bram Van Leer. Towards the ultimate conservative difference scheme. V. A second-order sequel to Godunov's method. *Journal of computational Physics*, 32(1):101–136, 1979.

Sergei Konstantinovich Godunov. A difference method for numerical calculation of discontinuous solutions of the equations of hydrodynamics. *Matematicheskii Sbornik*, 89(3):271–306, 1959.

Phillip Colella and Paul R Woodward. The piecewise parabolic method (PPM) for gas-dynamical simulations. *Journal of computational physics*, 54(1):174–201, 1984.

Ami Harten, Bjorn Engquist, Stanley Osher, and Sukumar R Chakravarthy. Uniformly high order accurate essentially non-oscillatory schemes, III. *Journal of Computational Physics*, 71(2):231–303, 1987. doi:10.1016/0021-9991(87)90031-3.

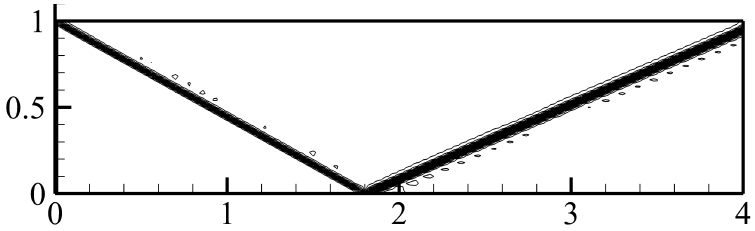

(a) WENO-FV with NCD

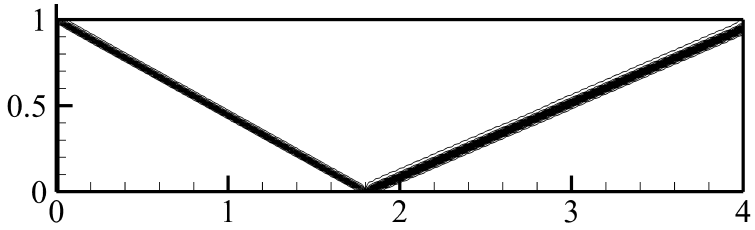

(b) WENO-FV with SCD

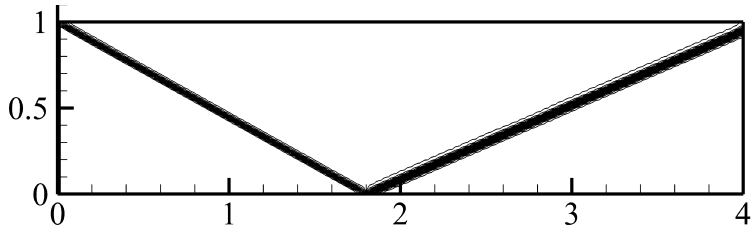

(c) WENO-FV with RCD

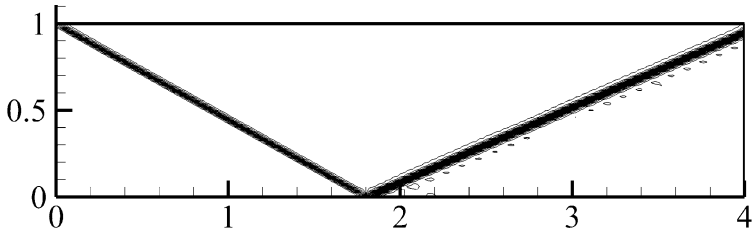

(d) WENO-FV with xCD

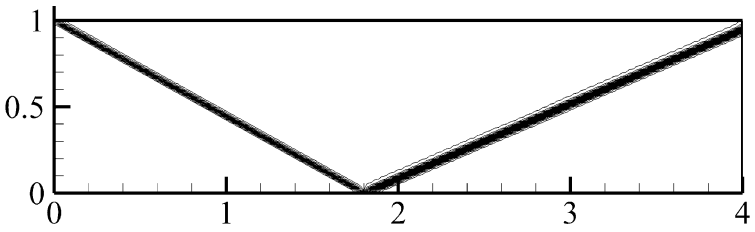

(e) WENO-FV with yCD

Figure 3: The density contours of the steady shock reflection on a plate at $t = 15$ calculated by the third-order WENO-FV scheme with different characteristic decomposition techniques. The mesh size is 1/50 and the density contours contain 30 equidistant contours from 1.1 to 2.7.

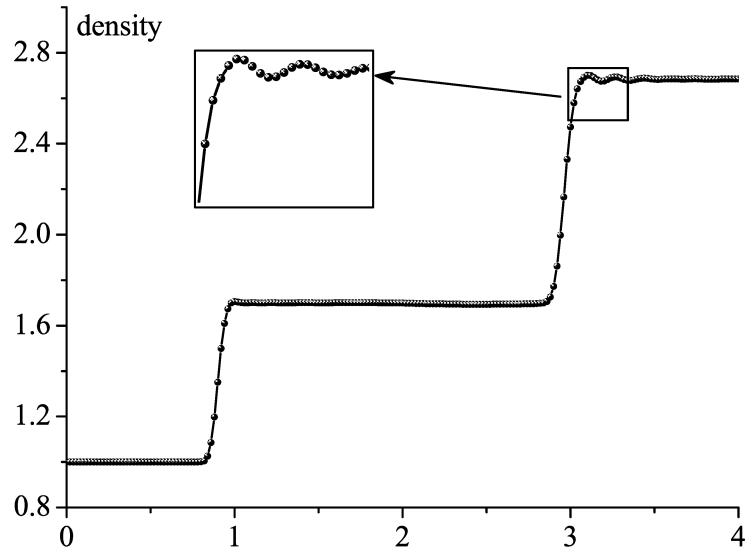

(a) WENO-FV with NCD

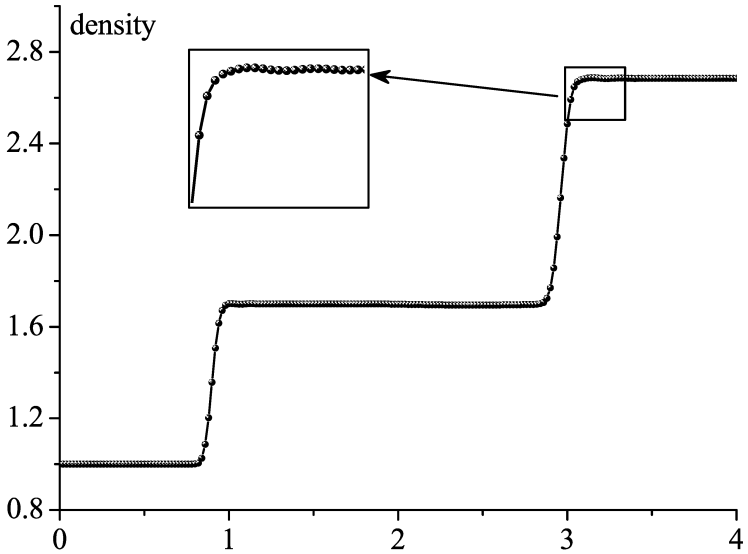

(b) WENO-FV with SCD

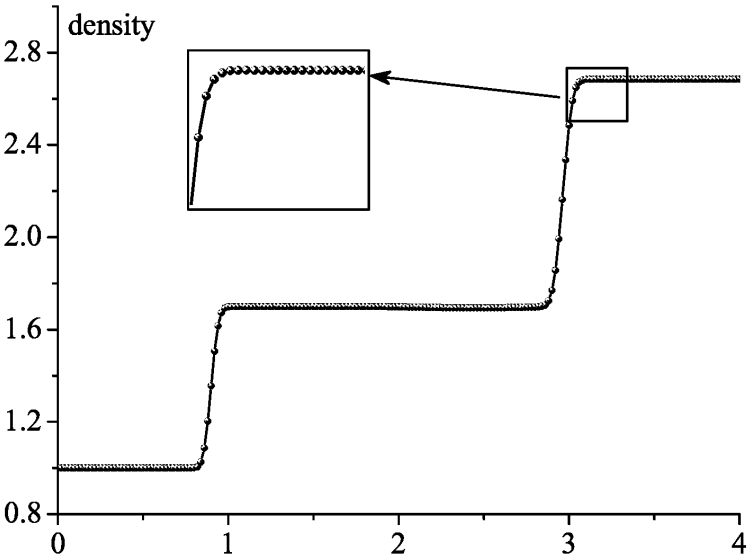

(c) WENO-FV with RCD

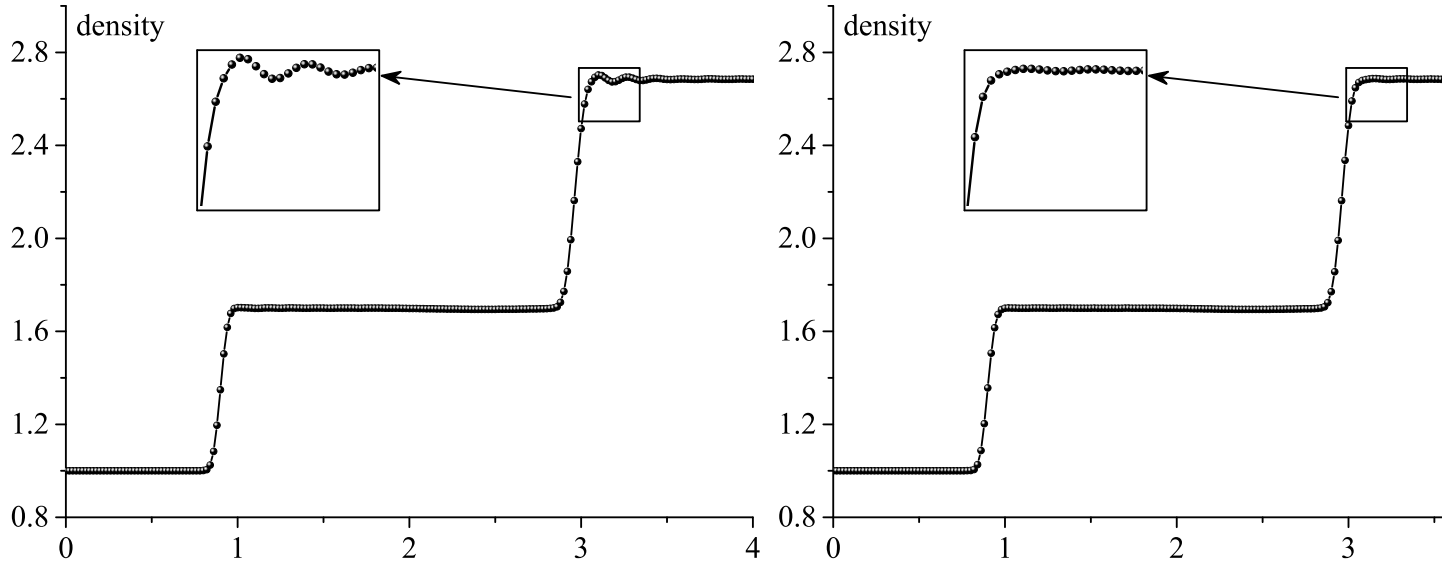

(d) WENO-FV with xCD (e) WENO-FV with yCD

Figure 4: The density profiles of the steady shock reflection on a plate along the line $y = 0.5$ at $t = 15$ calculated by the third-order WENO-FV scheme with different characteristic decomposition techniques.

Xu-Dong Liu, Stanley Osher, Tony Chan, et al. Weighted essentially non-oscillatory schemes. *Journal of computational physics*, 115(1):200–212, 1994.

Guang-Shan Jiang and Chi-Wang Shu. Efficient implementation of weighted ENO schemes. *Journal of Computational Physics*, 126(1):202–228, 1996. doi:10.1006/jcph.1996.0130.

Rafael Borges, Monique Carmona, Bruno Costa, and Wai Sun Don. An improved weighted essentially non-oscillatory scheme for hyperbolic conservation laws. *Journal of Computational Physics*, 227(6):3191–3211, 2008.

Doron Levy, Gabriella Puppo, and Giovanni Russo. Central WENO schemes for hyperbolic systems of conservation laws. *ESAIM: Mathematical Modelling and Numerical Analysis*, 33(3):547–571, 1999.

Doron Levy, Gabriella Puppo, and Giovanni Russo. A third order central WENO scheme for 2D conservation laws. *Applied Numerical Mathematics*, 33(1):415–422, 2000a.

Doron Levy, Gabriella Puppo, and Giovanni Russo. Compact central WENO schemes for multidimensional conservation laws. *SIAM Journal on Scientific Computing*, 22(2):656–672, 2000b.

Isabella Cravero, Matteo Semplice, and Giuseppe Visconti. Optimal definition of the nonlinear weights in multidimensional central WENOZ reconstructions. *SIAM Journal on Numerical Analysis*, 57(5):2328–2358, 2019.

Rémi Abgrall. On essentially non-oscillatory schemes on unstructured meshes: analysis and implementation. *Journal of Computational Physics*, 114(1):45–58, 1994.

Changqing Hu and Chi-Wang Shu. Weighted essentially non-oscillatory schemes on triangular meshes. *Journal of Computational Physics*, 150(1):97–127, 1999.

Michael Dumbser and Martin Käser. Arbitrary high order non-oscillatory finite volume schemes on unstructured meshes for linear hyperbolic systems. *Journal of Computational Physics*, 221(2):693–723, 2007.

Wm H Reed and TR Hill. Triangular mesh methods for the neutron transport equation. *Los Alamos Report LA-UR-73-479*, 1973.

Bernardo Cockburn and Chi-Wang Shu. TVB Runge-Kutta local projection discontinuous Galerkin finite element method for conservation laws. II. General framework. *Mathematics of computation*, 52(186):411–435, 1989.

Bernardo Cockburn, San-Yih Lin, and Chi-Wang Shu. TVB Runge-Kutta local projection discontinuous Galerkin finite element method for conservation laws. III: One-dimensional systems. *Journal of computational physics*, 84 (1):90–113, 1989.

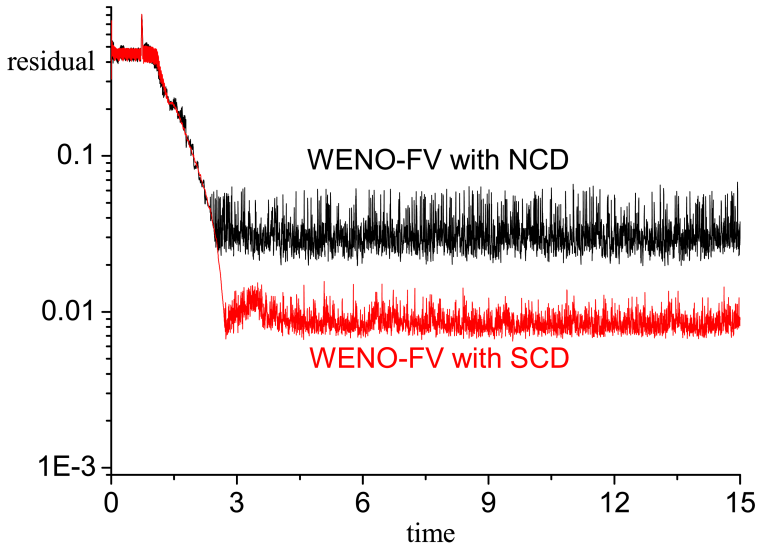

(a) WENO-FV with NCD and SCD

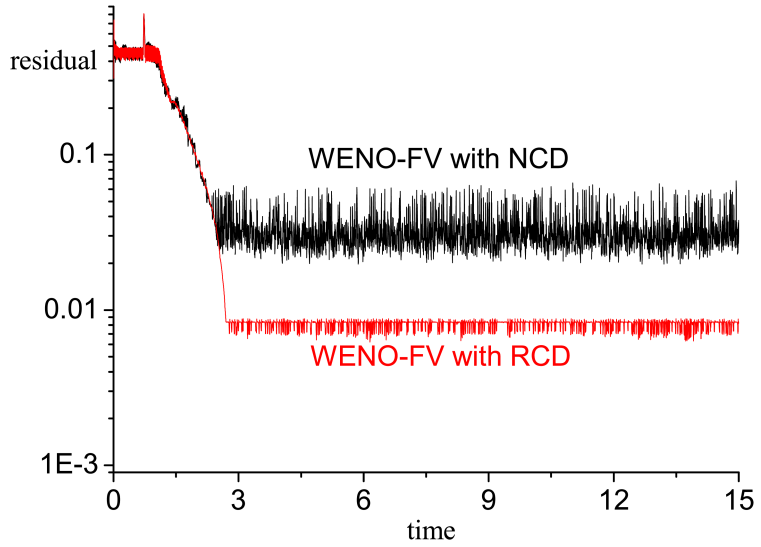

(b) WENO-FV with NCD and RCD

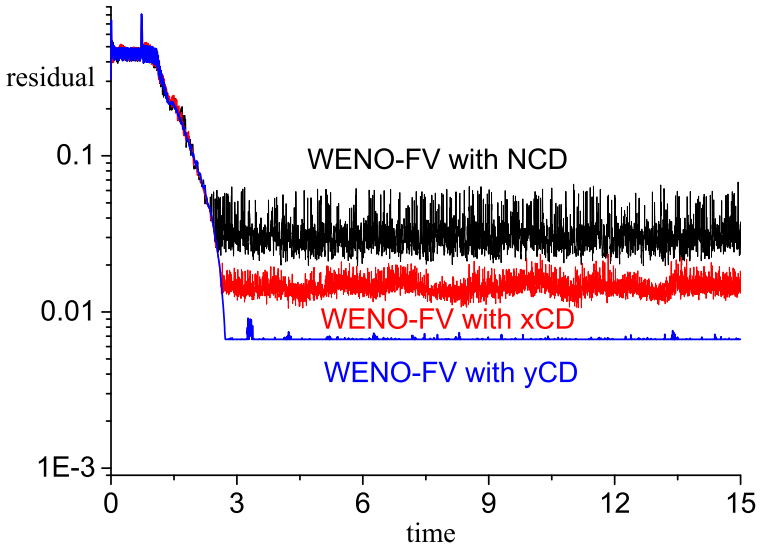

(c) WENO-FV with NCD, xcd and yCD

Figure 5: The maximum residual histories of the steady shock reflection calculated by the third-order WENO-FV scheme with different characteristic decomposition techniques.

Bernardo Cockburn, Suchung Hou, and Chi-Wang Shu. The Runge-Kutta local projection discontinuous Galerkin finite element method for conservation laws. IV. The multidimensional case. *Mathematics of Computation*, 54 (190):545–581, 1990.

Bernardo Cockburn and Chi-Wang Shu. The Runge-Kutta local projection discontinuous Galerkin finite element method for conservation laws. V: Multidimensional systems. *Journal of computational physics*, 141(2):199–224, 1998.

Jianxian Qiu and Chi-Wang Shu. Hermite WENO schemes and their application as limiters for Runge–Kutta discontinuous Galerkin method: One-dimensional case. *Journal of Computational Physics*, 193(1):115–135, 2004.

Jianxian Qiu and Chi-Wang Shu. Hermite WENO schemes and their application as limiters for Runge–Kutta discontinuous Galerkin method II: Two-dimensional case. *Computers & Fluids*, 34(6):642–663, 2005.

Xinghui Zhong and Chi-Wang Shu. A simple weighted essentially nonoscillatory limiter for Runge–Kutta discontinuous Galerkin methods. *Journal of Computational Physics*, 232(1):397–415, 2013.

Jun Zhu, Xinghui Zhong, Chi-Wang Shu, and Jianxian Qiu. Runge-Kutta discontinuous Galerkin method with a simple and compact Hermite WENO limiter. *Communications in Computational Physics*, 19(4):944–969, 2016.

Michael Dumbser, Dinshaw S Balsara, Eleuterio F Toro, and Claus-Dieter Munz. A unified framework for the construction of one-step finite volume and discontinuous Galerkin schemes on unstructured meshes. *Journal of Computational Physics*, 227(18):8209–8253, 2008. doi:10.1016/j.jcp.2008.05.025.

Michael Dumbser and Olindo Zanotti. Very high order $P_N P_M$ schemes on unstructured meshes for the resistive relativistic MHD equations. *Journal of Computational Physics*, 228(18):6991–7006, 2009.

Michael Dumbser. Arbitrary high order $P_N P_M$ schemes on unstructured meshes for the compressible Navier–Stokes equations. *Computers & Fluids*, 39(1):60–76, 2010.

Jianxian Qiu and Chi-Wang Shu. On the construction, comparison, and local characteristic decomposition for high-order central weno schemes. *Journal of Computational Physics*, 183(1):187–209, 2002.

Chi-Wang Shu and Stanley Osher. Efficient implementation of essentially non-oscillatory shock-capturing schemes. *Journal of Computational Physics*, 77:439–471, 1988.

Yu-Xin Ren, Hanxin Zhang, et al. A characteristic-wise hybrid compact-weno scheme for solving hyperbolic conservation laws. *Journal of Computational Physics*, 192(2):365–386, 2003.

Gabriella Puppo. Adaptive application of characteristic projection for central schemes. In *Hyperbolic problems: theory, numerics, applications*, pages 819–829. Springer, 2003.

Gabriella Puppo and Matteo Semplice. Numerical entropy and adaptivity for finite volume schemes. *Communications in Computational Physics*, 10(5):1132–1160, 2011.

Gang Li and Jianxian Qiu. Hybrid weighted essentially non-oscillatory schemes with different indicators. *Journal of Computational Physics*, 229(21):8105–8129, 2010.

Jun Peng, Chuanlei Zhai, Guoxi Ni, Heng Yong, and Yiqing Shen. An adaptive characteristic-wise reconstruction weno-z scheme for gas dynamic euler equations. *Computers & Fluids*, 179:34–51, 2019.

Dinshaw S Balsara, Tobias Rumpf, Michael Dumbser, and Claus-Dieter Munz. Efficient, high accuracy ADER-WENO schemes for hydrodynamics and divergence-free magnetohydrodynamics. *Journal of Computational Physics*, 228 (7):2480–2516, 2009.

Eleuterio F Toro. *Riemann solvers and numerical methods for fluid dynamics: a practical introduction*. Springer Science & Business Media, 2013.

Paul Woodward and Phillip Colella. The numerical simulation of two-dimensional fluid flow with strong shocks. *Journal of computational physics*, 54(1):115–173, 1984.

HC Yee, RF Warming, and A Harten. Implicit total variation diminishing (TVD) schemes for steady-state calculations. *Journal of Computational Physics*, 57(3):327–360, 1985.

Jun Zhu and Chi-Wang Shu. Numerical study on the convergence to steady state solutions of a new class of high order WENO schemes. *Journal of Computational Physics*, 349:80–96, 2017.